Chemical Engineering Journal 332 (2018) 24–32

Contents lists available at ScienceDirect

Chemical Engineering Journal

journal homepage: www.elsevier.com/locate/cej

Adsorption of CO_2 on mixed oxides derived from hydrotalcites at several temperatures and high pressures

S.I. Garcés-Polo[a,1], J. Villarroel-Rocha[c], K. Sapag[c], S.A. Korili[a,b], A. Gil[a,b,*]

[a] Departamento de Química Aplicada, Edificio de los Acebos, Universidad Pública de Navarra, Campus de Arrosadía, 31006 Pamplona, Spain
[b] Instituto de Materiales Avanzados – INAMAT, Universidad Pública de Navarra, Campus de Arrosadía, 31006 Pamplona, Spain
[c] Laboratorio de Sólidos Porosos, INFAP, CONICET-Universidad Nacional de San Luis, Chacabuco, 917, 5700 San Luis, Argentina

GRAPHICAL ABSTRACT

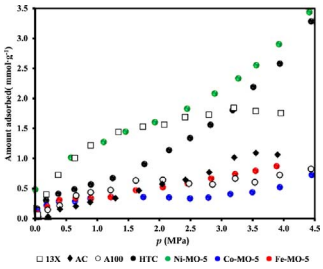

ARTICLE INFO

Keywords:
CO_2 adsorption
High pressure adsorption
High temperature adsorption
Hydrotalcite

ABSTRACT

The adsorption of CO_2 on Co, Fe and Ni mixed oxides derived from a commercial hydrotalcite and calcined at 500 °C was measured at several temperatures and pressures. Two types of experiments were considered in this work. In the first one, the adsorption temperatures were 25, 35 and 50 °C, with pressures of up to 1000 kPa. In the second, the adsorption temperature was 300 °C and the pressure up to 4400 kPa. The results obtained were compared with those found for four commercial microporous materials, namely the zeolite 13X, the MOF Basolite A100, an activated carbon and a synthetic alumina pillared clay. The microporous materials showed a higher CO_2 adsorption capacity, from 4.54 to 6.94 mmol·g^{-1}, than the mixed oxides, up to 1.44 mmol·g^{-1}, at 25 °C and up to 1000 kPa. The calcined hydrotalcite and the Ni mixed oxide presented the highest CO_2 adsorption capacity at 300 °C, 3.28 and 3.44 mmol·g^{-1} at 4400 kPa, whereas the rest of materials gave values of up to 1.75 mmol·g^{-1}. Ni mixed oxide showed sorption capacity considerably higher than those reported in the literature for hydrotalcite based materials under similar conditions.

1. Introduction

The capture and storage of CO_2 is considered to be a potential strategy in the portfolio of mitigation actions required to stabilize atmospheric greenhouse gas concentrations [1]. Precombustion, postcombustion and oxyfuel combustion are the three main processes for CO_2 capture in industrial and power plant applications. In this context, gas-solid adsorption is one of the technological areas currently in use and continuously being developed [2].

The Sorption-Enhanced Reaction Process (SERP) is an emerging concept in precombustion systems. In this process, CO_2 capture is performed *in situ* by combining chemical reaction and separation of the reaction products in the same operation [3]. These processes combine adsorption with conventional hydrogen production reactions (WGS:

* Corresponding author at: Departamento de Química Aplicada, Edificio de los Acebos, Universidad Pública de Navarra, Campus de Arrosadía, 31006 Pamplona, Spain.
E-mail address: andoni@unavarra.es (A. Gil).
[1] Present address: Facultad de Ingeniería, Universidad Libre, Bosque Popular, 111061 Bogotá, Colombia.

http://dx.doi.org/10.1016/j.cej.2017.09.056
Received 17 July 2017; Received in revised form 7 September 2017; Accepted 8 September 2017
Available online 09 September 2017
1385-8947/

water gas shift and SRM: *steam reforming of methane*) and, depending on the reaction involved, the processes are referred to as SEWGS or SESRM. In both processes, the reactants are fed into a reactor containing a mixture of catalyst and adsorbent at operating conditions of 300–500 °C and 400–2000 kPa (SESRM) or 200–400 °C and 100–2800 kPa (SEWGS). The reaction and removal of CO_2 from the reaction zone occur simultaneously, thereby producing high purity hydrogen. Finally, the adsorbent is regenerated *in situ* using the principles of Pressure Swing Adsorption (PSA) or Thermal Swing Adsorption (TSA) at reaction temperature [3–5].

All current routes for CO_2 capture include several operating conditions. Postcombustion technologies, for instance, can be implemented at temperatures lower than 100 °C, atmospheric pressure and low CO_2 concentrations (< 15%), or directly from the gas stream at 150–400 °C. Similarly, precombustion processes are carried out at temperatures ranging from 40 to 250 °C and a pressure of 3 MPa [6].

The wide range of operating conditions for these technologies leads to the use of a variety of specific adsorbents for each application. Carbonaceous materials, such as activated carbons, exhibit the best adsorption capacity at temperatures lower than 50 °C and pressures higher than 100 kPa, with the amount adsorbed decreasing strongly at higher temperatures [7–10]. Zeolites show the best CO_2 adsorption capacity at low temperatures (0–100 °C) and in a wide range of pressures [7,11,12]. MOF materials, in turn, show a high adsorption capacity at room temperature and high pressures (about 3.5 MPa), although their capacity decreases with increasing temperature and in the presence of moisture and impurities [6,13]. In general, the use of physisorbent materials is limited to SERP technologies and postcombustion at intermediate and high temperatures, between 200 and 400 °C. Chemisorbent materials have gained interest due their high and reversible CO_2 adsorption capacity. Among this group of materials, alkali and alkaline earth metal oxides, double oxides, hydrotalcite compounds and their derived oxides obtained by calcination have attracted increasing attention. Indeed, several reviews have made a detailed comparison of these materials, highlighting the general characteristics of these adsorbents and their maximum adsorption capacity [6,8,14,15]. Specifically, hydrotalcites have been identified as chemisorbents for use at intermediate temperatures [15].

The aim of this work was to evaluate the CO_2 adsorption capacity of Co, Fe and Ni mixed oxides obtained from aqueous impregnation a commercial hydrotalcite as potential adsorbents in precombustion processes. The results are compared with four microporous materials selected from previous studies. Information related to several materials and their CO_2 adsorption capacity under several conditions of temperature and pressures are given in Table S1 of the Supporting Information. To the best of our knowledge, there are very few reports of CO_2 adsorption on mixed oxides derived from hydrotalcites under the experimental conditions studied in this work, high temperatures and pressures.

2. Experimental

2.1. Materials, reagents and gases

Materials and reagents used for the synthesis of mixed oxides derived from the hydrotalcite were: $Co(NO_3)_2{\cdot}6H_2O$ (Panreac, PA), $Fe(NO_3)_3{\cdot}6H_2O$ (Sigma-Aldrich), $Ni(NO_3)_2{\cdot}6H_2O$ (Panreac, PA) and $Mg_6Al_2(CO_3)(OH)_{16}{\cdot}4H_2O$ (Sigma-Aldrich). Four commercial adsorbents were used as reference: a zeolite 13X (Sigma-Aldrich), a MOF (Basolite A100 (MIL-53-Al) purchased from Sigma-Aldrich), an activated carbon (AC; Sigma-Aldrich, Darko KB-B) and a synthetic alumina pillared clay (Al-PILC) [16]. Pure oxides (NiO, 99.999%, Sigma-Aldrich; Co_3O_4, 99.9985%, Strem Chemicals; Fe_2O_3, 99.99%, Sigma-Aldrich) are also included for comparison in the characterization section. Carbon dioxide (AGA, 99,996%), nitrogen (Air Liquide, 99.999%) and helium (Air Liquide, 99.999%) were also used.

2.2. Preparation of the materials

The materials selected in this study include three mixed Co, Fe and Ni oxides with a content of 5 wt%, Ni-MO-5, Fe-MO-5 and Co-MO-5, obtained from a commercial hydrotalcite, HT. These oxides were initially prepared from HT previously calcined at 500 °C and impregnated with aqueous solutions of the corresponding nitrate salt. The resulting material was then dried at 100 °C and finally calcined at 500 °C for 4 h in order to obtain the mixed oxides.

2.3. Characterization techniques

In order to characterize the crystalline phases of the mixed oxides, the powder X-ray diffraction (PXRD) patterns were recorded using a Siemens D-5000 diffractometer equipped with a Ni-filtered Cu Kα radiation source (λ = 0.1548 nm). The working conditions used were 30 mA, 40 kV and a scanning rate of 2° (2θ)/min from 4 to 90°.

The textural properties of the mixed oxides in the micro-mesoporous region were obtained from N_2 adsorption-desorption experiments at −196 °C using a static volumetric apparatus (Micromeritics ASAP 2010 adsorption analyzer). Prior to the adsorption measurements, 0.3 g of sample was degassed at 200 °C for 24 h at pressures lower than 0.133 Pa. In the case of HT, the sample was pretreated at 100 °C. The textural characteristics of the meso-macroporous region were also obtained by Hg intrusion-extrusion experiments using an intrusion porosimeter apparatus (Micromeritics AUTOPORE-III). Prior to analysis, 0.5 g of sample was degassed at room temperature up to 7 Pa. Hg was introduced at a fill pressure of 2 kPa. The analysis at low pressure was performed from 3.4 to 206 kPa, followed by high pressure measurements up to 413 MPa, thus allowing the identification of pore sizes from 360 μm to 3 nm.

Temperature-programmed reduction (TPR) studies were performed using a Micromeritics TPR/TPD 2900 equipment instrument. TPR tests were then carried out from room temperature to 1000 °C, at a heating rate of 10 °C min^{-1}, under a total flow of 30 cm^3 min^{-1} (5% H_2 in Ar, Praxair).

The thermogravimetric analysis of Ni-MO-5, before and after CO_2 adsorption at 300 °C, was performed using a Hi-Res TGA2950 apparatus from TA-Instruments. The measurements were carried out at a heating rate of 10 °C min^{-1} from room temperature to 800 °C under nitrogen atmosphere and a flow of 60 cm^3/min.

2.4. CO_2 adsorption experiments

Carbon dioxide adsorption experiments at 25, 35 and 50 °C were performed using a static volumetric apparatus (Micromeritics ASAP 2050) at pressures up to 1000 kPa. The samples (0.5 g) were previously degassed under vacuum at 200 °C for 24 h, except for the HT material, which was degassed at 100 °C to avoid any structure modification. The adsorption temperature was controlled using a circulating thermostatic bath containing ethylene glycol solution as the heat-transfer medium.

Adsorption experiments at 300 °C and pressures up to 4400 kPa were performed using a different static volumetric apparatus (VTI HPA-100). The degassing conditions were similar to those at low temperatures. The density of CO_2 gas under these experimental conditions was obtained using REFPROP v. 8.0 software, which contains the NIST *Standard Reference Database*. The excess CO_2 adsorption isotherms were calculated using these density data.

3. Results and discussion

3.1. Characterization of materials

3.1.1. Powder X-ray diffraction

Diffraction patterns for the commercial hydrotalcite (HT), the calcined hydrotalcite (HTC) and the mixed oxides are shown in Fig. 1(a,

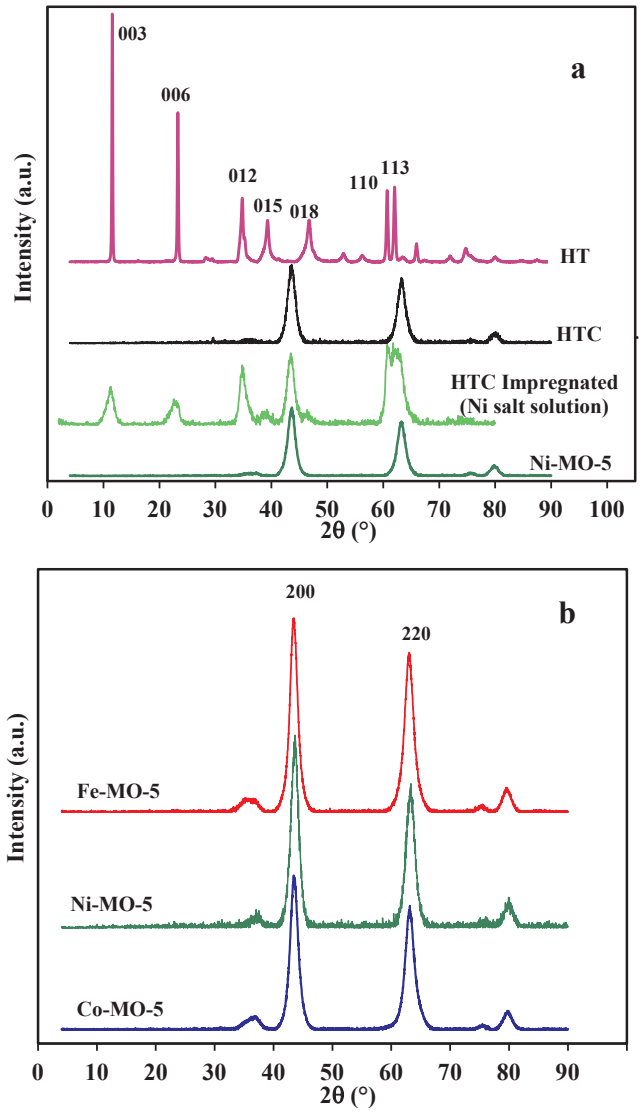

Fig. 1. PXRD patterns of HT, HTC, HTC impregnated with Ni salt solution compared with Ni-MO-5 (a) and Co-, Fe-, and Ni-mixed oxides (b).

b). The starting material HT exhibited characteristic reflections of a typical hydrotalcite structure with sharp and symmetrical diffraction peaks at low and high 2θ values and asymmetrical and less intense lines at intermediate values [17]. After calcination of the hydrotalcite, the diffraction profile was found to be modified by the thermal treatment. In the current case, at 500 °C, the original layered structure of HT collapsed and two new peaks of highest intensity being found at around 43 and 63°, related to the periclase phase MgO (JCPDS file 45-0946). This behavior is due to the fact that calcination at 500 °C destroyed the layered structure of HT. The spinel phase of $MgAl_2O_4$ was not clearly identified due to the calcination temperature used [17,18]. In addition, well dispersed or amorphous spinel phases of mixed oxides with aluminum ions could also be formed but not detected by XRD [19]. A comparison of the diffraction profiles for the HTC sample and MgO standard showed a slight shift in the peaks to higher angles in the case of the HTC sample. This could reflect a substitution of Al^{3+} ions in the MgO crystal lattice to form solid solutions of $Mg_{0.7}Al_{0.3}O_{1.15}$ at 500 °C [20], with Al^{3+} ions being found at the highest concentration at the surface of the oxide Mg-Al-O [21].

After impregnation of HTC with an aqueous metal nitrate solution to incorporate the metal, the layer structure of the support was recovered, as can be seen in Fig. 1a. Wider and less intense diffraction lines compared with the synthetic HT can be seen. A loss of resolution in planes (1 1 0) and (1 1 3) suggests the formation of a new, less-ordered structure containing a lower amount of HT due to the presence of mixed oxides and periclase phases. Further calcination of the material gives rise to formation of the final compound (i.e., Ni-MO-5 in Fig. 1a), which contains only periclase and mixed-oxide phases.

The PXRD patterns of all mixed oxides obtained, Co-MO-5, Fe-MO-5 and Ni-MO-5, are shown in Fig. 1b. In general, the three materials exhibit crystalline structures similar to that for the MgO pattern. In addition, a combination of several mixed oxides was identified according to the ICDD files (see Tables S2–S4 in the Supporting Information). The diffraction peaks observed for Ni-MO-5 correspond to NiO, MgO, $Mg_{0.4}Ni_{0.6}$ and to solid solutions of $MgNiO_2$/MgO·NiO, the latter being difficult to differentiate from the rest due to its high dispersion and low concentration. A similar PXRD pattern for Ni mixed oxides derived from hydrotalcite has been reported [22,23]. Other authors have also suggested the probable incorporation of Ni^{2+} and Al^{3+} into the cubic lattice to form the mixed oxide Mg(Ni,Al)O [17,24].

Regarding the mixed cobalt oxides derived from hydrotalcite, Co species can interact strongly with Mg^{2+} and Al^{3+} species to form the solid solutions periclase Mg(CoAl)O and spinels, which are very difficult to distinguish [25–27]. This fact could explain the broad diffraction peaks found for Co-OM-5, with $(Mg_xCo_{1-x})(Mg_yCo_{1-y})O_4$, Co_3O_4, Co_2AlO_4 spinel phases and $MgAl_2O_4$ only being identified at 37°, possibly because of the low cobalt content. The formation of Co_3O_4 in this material is expected at 500 °C as Co^{2+} ions are easily oxidizable and Co_3O_4 is thermodynamically more stable in air than CoO [20].

Similar to the Ni and Co mixed oxides, the MgO phase was also identified in Fe-MO-5, and the $(MgO)_{0.91}(FeO)_{0.09}$ phase was assigned at the same diffraction angles as the MgO pattern [21,28]. Although the hematite phase Fe_2O_3 may also be present, it was not clearly identifiable, possibly due to the fact that the low iron content interacts strongly with the MgO phase.

3.1.2. Textural analysis

The nitrogen adsorption-desorption isotherms for HT, HTC and the mixed oxides are shown in Fig. 2. The isotherms were identified as type II (a or b) according to the IUPAC classification [29,30]. It can be seen that the volume adsorbed at high p/p^0 values increased rapidly, thus suggesting the presence of large mesopores and macropores. These samples can therefore be categorized as meso-macroporous materials. An H3-type hysteresis loop characteristic of non-rigid aggregates of plate-like particles was observed for all materials [30]. In addition, a small hysteresis loop was found for HTC, thus suggesting the same

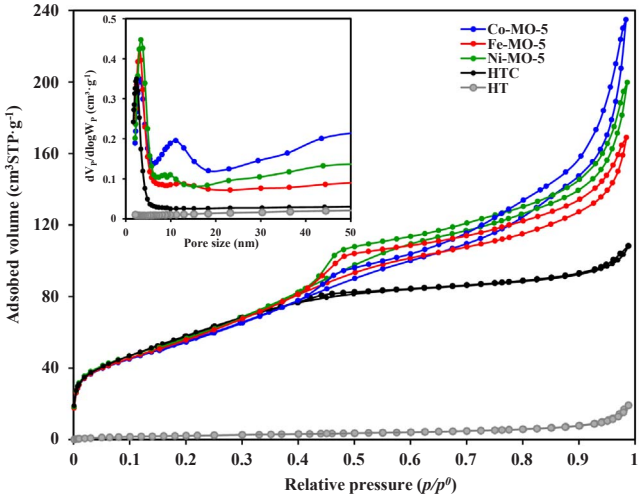

Fig. 2. N_2 adsorption-desorption isotherms at −196 °C and pore-size distributions using the BJH method.

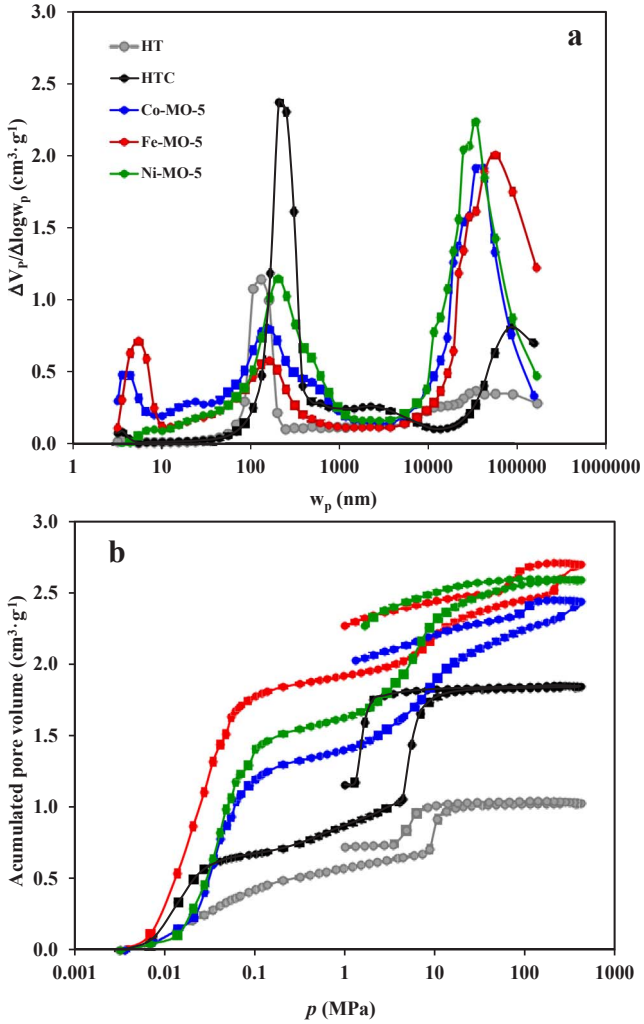

Fig. 3. Pore-size distributions by Hg intrusion porosimetry (a) and Hg intrusion-extrusion curves (b).

mechanism for filling and emptying of the pores. An estimation of the mesopore size distribution, which was obtained by applying the BJH method to the adsorption data, is provided as an insert to Fig. 2 [31]. All the mixed oxides exhibited narrow distributions in the lower range of mesopore size (2–6 nm). A small distribution can also be observed at higher pore sizes up to 15 nm. In the case of HT, this distribution suggests that the amount of pores in the mesopore size region is negligible.

Additional textural information concerning the macroporosity of the materials was obtained by Hg intrusion porosimetry (see Fig. 3). The HT sample exhibited a well-defined pore-size distribution with a maximum around 130 nm and a wider distribution in the range of larger macropores. The HTC sample exhibited an increase in macroporosity toward a pore size of 200 nm, along with a small mesopore contribution, from 2 to 15 nm. As regards the mixed oxides, a trimodal distribution containing mesopores and macropores, with a more pronounced distribution in the region from 2 to 15 nm, was obtained, especially in Fe-MO-5 (5.5 nm) and Co-MO-5 (3.6 nm). In the intermediate region (50–750 nm), a comparison of HTC with the mixed oxides showed a reduction of this type of pore in the oxides due to the incorporation of Co, Fe and Ni. The formation of mixed oxides and spinels leads to the creation of macropores with a size of about $34x10^3$ nm in Co-MO-5 and Ni-MO-5 and 56 × 10^3 nm in the case of Fe-MO-5. All these results indicate a regular and well-defined distribution of the porosity in the meso-macroporous region, with a negligible presence of microporosity.

The textural properties obtained from N_2 adsorption at −196 °C and Hg intrusion data are summarized in Table 1. The specific surface area (S_{BET}) and total pore volume (V_P) were calculated according to established procedures published previously [16]. The total pore volume (V_{Hg}), specific surface area (S_{Hg}), bulk density (ρ_B) and apparent density (ρ) were obtained by Hg intrusion experiments. The S_{BET} and V_P values for the HT material are very low because their structure remains unchanged after thermal treatment at 200 °C [32]. In the case of the HTC sample, the thermal treatment at 500 °C increased the specific surface area up to 220 $m^2 \cdot g^{-1}$. A cratering process occurs in the material at this temperature, with this process generating porosity due to interstitial water loss, decomposition of interlayer CO_3^{2-} and dehydroxylation of brucite sheets [33]. In addition, formation of the mixture of an MgO phase and a mixed oxide could lead to an increase in the total pore volume. The increase in S_{BET} is quite similar for Co and Fe mixed oxides, reaching values of about 200 $m^2 \cdot g^{-1}$. In the case of the Ni-MO-5 sample, the S_{BET} is higher than that of Co and Fe mixed oxides due to the presence of spinel phases.

3.1.3. Temperature-programmed reduction

The TPR profiles of the three mixed oxides are presented in Fig. 4. The profiles for the pure oxides are also included for comparison. All materials exhibited two reduction peaks: the first one appearing between 200 and 600 °C and the other between 600 and 1100 °C. In the Ni-MO-5 sample, the first stage at around 480 °C is related to the initial NiO reduction, which is segregated from a subsequent reduction of the oxide occupying surface centers of the MgO structure [34]. The second peak at higher temperatures (877 °C) corresponds to the interaction between the NiO and MgO structures. It was assigned to the Ni^{2+} ions located inside the MgO lattice, which form a Ni/MgO and mixed oxides solid solution that is difficult to reduce and is promoted by calcination of the support, HTC. This behavior has also been described previously by other authors [22,35,36].

The reduction profile for the cobalt species in Co-MO-5 includes a first peak at 391 °C that can be related to the reduction of pure Co_3O_4 to metallic Co. The shoulder observed at about 300 °C in this region is also related to the reduction of Co_3O_4 in two stages: $Co^{3+} \rightarrow Co^{2+} \rightarrow Co^0$ [37]. The reduction peak at high temperature is due to the reduction of Co^{2+} species present in the mixed oxides and cobalt spinels. Specifically, the species contained in the spinel Co_2AlO_4 presents a low accessibility to H_2 due to the presence of Al^{3+} ions that polarize the Co-O bonds [27,37].

Table 1
Textural properties derived from N_2 adsorption at −196 °C and Hg intrusion porosimetry.

Sample	S_{BET} ($m^2 \cdot g^{-1}$)	V_P ($cm^3 \cdot g^{-1}$)	V_{Hg} ($cm^3 \cdot g^{-1}$)	S_{Hg} ($m^2 \cdot g^{-1}$)	ρ_B ($g \cdot cm^{-3}$)	ρ ($g \cdot cm^{-3}$)	Porosity[a] (%)
HT	9	0.03	1.03	19	0.626	1.758	64
HTC	220	0.19	1.85	31	0.425	1.976	78
Ni-MO-5	210	0.31	2.59	48	0.328	2.182	85
Co-MO-5	195	0.36	2.44	198	0.368	3.579	90
Fe-MO-5	200	0.26	2.70	217	0.346	5.271	93

[a] Porosity = $\frac{V_{Hg}}{1/\rho_B} \times 100$.

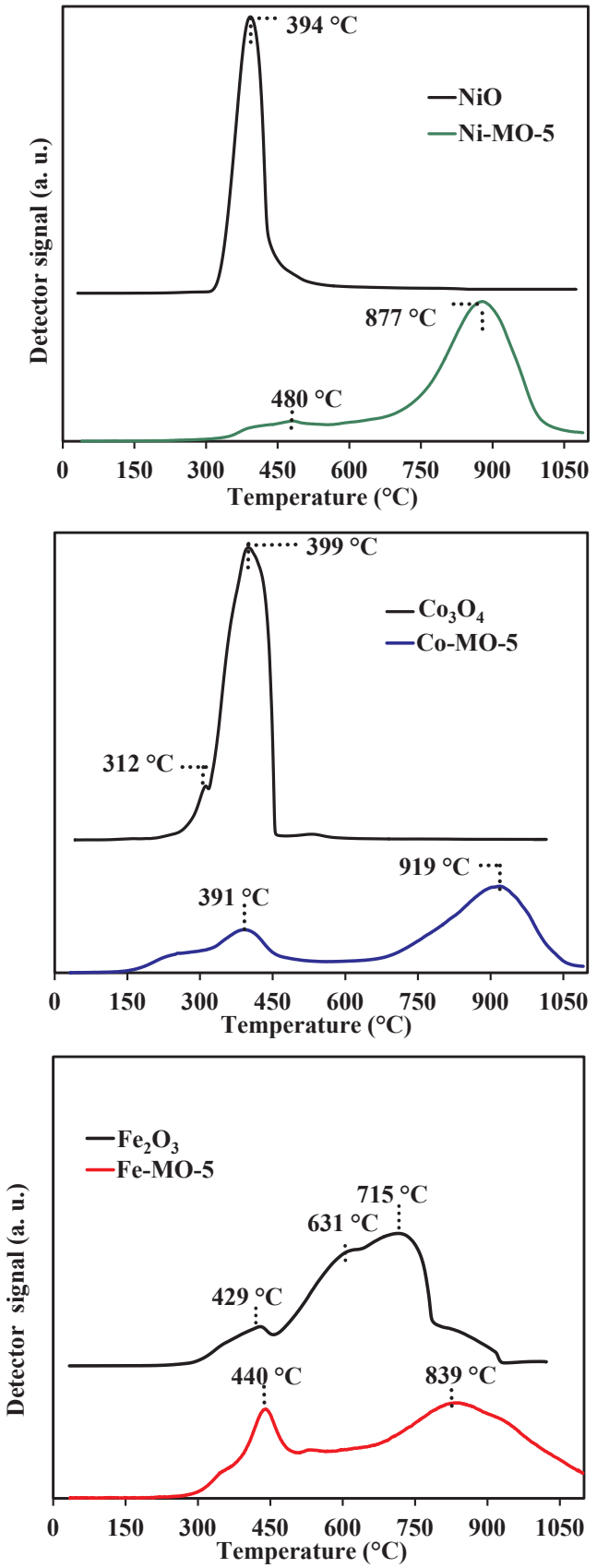

Fig. 4. TPR profiles of Ni-MO-5, Co-MO-5 and Fe-MO-5.

The two reduction stages exhibited by Fe-MO-5 confirm the existence of several iron species. This reduction behavior is similar to the pattern for Fe_2O_3 but with reduction temperatures shifted to higher temperatures, thus suggesting the presence of Mg^{2+} and Al^{3+} ions [38]. The first peak involves the reduction of Fe_2O_3 to Fe^0 in the presence of MgO, and part of the mixed oxide, Mg-Fe-O and Mg-Fe-Al-O. The second stage continues the reduction of mixed oxides to metallic iron in the presence of MgO. These reactions have been described by Ge at al. [21] for this type of mixed oxide.

3.2. CO_2 adsorption at low temperatures and high pressures

The CO_2 adsorption capacity of the hydrotalcite-based Fe, Co and Ni mixed oxides at 25, 35 and 50 °C and pressures up to 1000 kPa are shown in Fig. 5. The results were compared with those obtained for four microporous materials, HT and HTC. In all cases, the amount of CO_2 adsorbed decreased with increasing adsorption temperature, which could be related to a physical interaction between the surface of the adsorbents and CO_2. The adsorption capacity at three pressures, including the postcombustion conditions of 15 kPa [15,39], 100 kPa and the highest pressure evaluated 1000 kPa, at 25, 35 and 50 °C, are summarized in Fig. 6. It can be seen that the materials 13X, A100 and AC exhibited the highest adsorption capacities. Zeolites, MOFs and activated carbons are widely used for CO_2 adsorption at temperatures lower than 200 °C and in a wide range of pressures [15,40]. In general, the performance of these materials is related to their porous structure: size, shape, pore size distribution and high specific surface area; and the interactions between the surface and CO_2 molecules [16,41–43]. In the case of Al-PILC, the porous structure and moderate specific surface area, about 200 $m^2 \cdot g^{-1}$, have a negligible effect on the adsorption capacity under these experimental conditions.

The adsorption results found for the HT sample at 25 °C are worth discussing further as this material does not undergo any structural changes at this temperature. It can clearly be seen from the results included in Fig. 6 that this material has a higher adsorption capacity than the mixed oxides at pressures lower than 100 kPa. As such, heat treatment improves the textural properties but not the CO_2 adsorption capacity. This result can be explained in terms of the interlaminar and surface structure of HT, which results in a surface accessible to CO_2 molecules, and the fact that H_2O molecules promote CO_2 adsorption [44]. Similarly, thermal treatment of the hydrotalcites produces two effects. The first effect is the generation of holes, channels and micropores, which leads to a higher pore volume and specific surface area, thus increasing the number of sites available for CO_2 adsorption. The second effect is a reduction in the basal space due to the total or partial collapse of the layered structure to form the mixed oxides [22,45]. The opposite behavior was found at higher pressures, with the amount of CO_2 adsorbed being higher in HTC and the mixed oxides than in synthetic HT, thus suggesting that the compositions and structures of the materials do not result in marked differences in their adsorption capacity. In the case of Co-MO-5, the presence of spinel might be responsible for the decrease of CO_2 adsorption capacity. A similar behavior was reported for a niquel mixed oxide sample containing a spinel phase [22]. At higher pressures, the amount of CO_2 adsorbed was higher in HTC and mixed oxides than in the synthetic HT, indicating that the differences in textural characteristics of the materials did not significantly modify the adsorption capacity.

With regard to the microporous adsorbents, in the case of 13X the CO_2 adsorption capacities at 100 and 1000 kPa and low temperatures were close to those reported in the literature [11,46]. A comparison of the results for 13X and AC showed that, at pressures lower than 200 kPa and temperatures of 25 and 35 °C, AC exhibited a lower adsorption capacity (1.71 and 1.39 $mmol \cdot g^{-1}$, at 100 kPa) than 13X (4.55 and 4.28, at 100 kPa). However, this behavior is reversed at pressures higher than 600 kPa. Thus, at 1000 kPa and temperatures of 25 and 35 °C, the adsorption capacity of AC is 6.94 and 6.07 $mmol \cdot g^{-1}$, and the

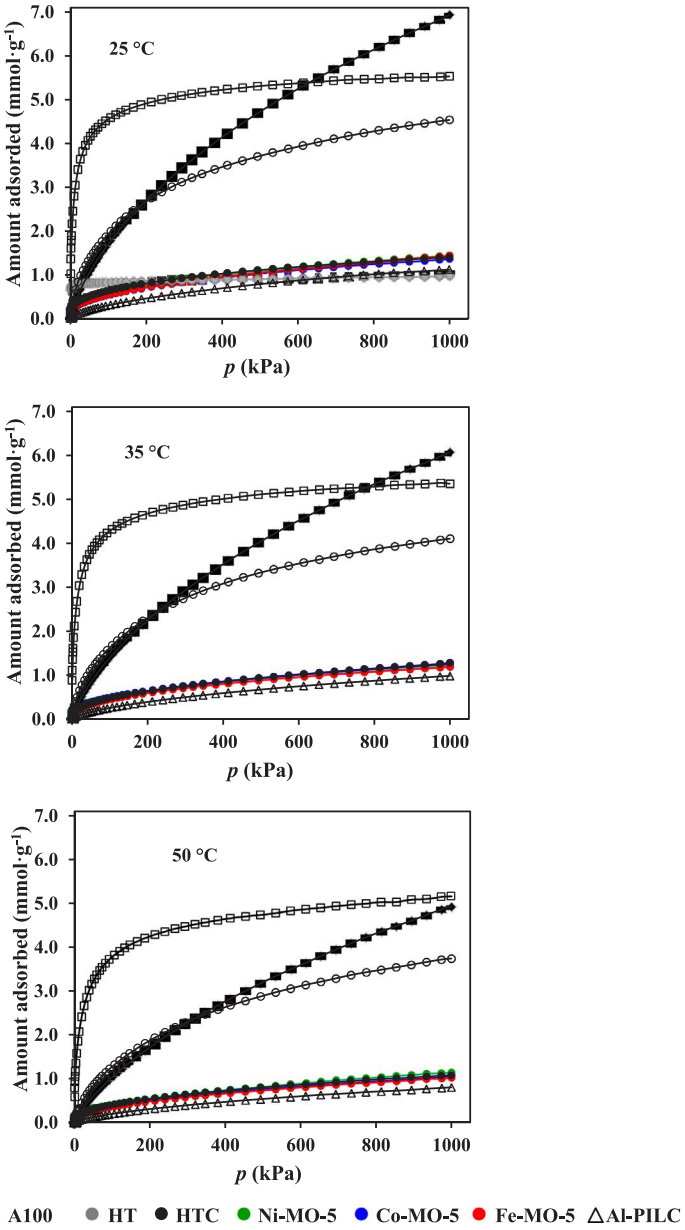

Fig. 5. CO_2 adsorption at 25, 35, 50 °C and pressures up to 1000 kPa.

adsorption capacity of 13X is 5.53 and 5.36 mmol·g^{-1}. At 50 °C, the amount of CO_2 adsorbed by the AC adsorbent is lower than for zeolites over the whole pressure range. Similarly, the CO_2 adsorption capacities at 25 and 35 °C and pressures up to 1000 kPa are in good accord with those found by Mu and Walton [9], with A100 showing a lower adsorption capacity than 13X and AC. At 1000 kPa, the amount adsorbed by this material is between 3.74 (50 °C) and 5.17 mmol·g^{-1} (25 °C). Al-PILC exhibited the lowest CO_2 adsorption capacities, with a maximum value of 1.12 mmol·g^{-1} at 25 °C and 1000 kPa. This result is in accord to the only value reported in the literature to date [47] (see Table S1 in Supporting Information). In general, the materials derived from hydrotalcite and Al-PILC exhibited a low CO_2 adsorption capacity at low temperatures and pressures up 1000 kPa. The enhanced adsorption capacity of the hydrotalcite and mixed oxides materials at intermediate and high temperatures is well-known in the literature (see Table S1).

3.3. CO_2 adsorption at 300°C and high pressures

The CO_2 adsorption capacities of the materials at 300 °C and pressures up to 4400 kPa are represented in Fig. 7 and summarized in Table 2. The results obtained reveal the effect of temperature and pressure in each type of material. Thus, a marked increase in the CO_2 adsorption, especially at high pressures, was observed for Ni-MO-5 and HTC, which clearly outperformed the other materials evaluated. This behavior is more moderate for Co-MO-5 and Fe-MO-5. It is evident that CO_2 adsorption in the case of AC and A100 mainly follows a physisorption process since their capacities decreased notably compared to the results obtained at low temperatures. The adsorption values for 13X are higher than for the other microporous materials selected. In the range of 0.6 to 1.7 MPa, a sort of knee is formed in which the adsorption capacities are close to the values obtained with Ni-MO-5. This could suggest that, despite the high temperature, the optimal adsorption capacity is located in this pressure range. In the case of zeolite materials, CO_2 adsorption involves physisorption and chemisorption at high and moderate temperatures. Specifically, CO_2 capture in zeolites is influenced by their textural properties, the high basicity of the surface, the number of cations and their distribution in the cavities, the Si/Al ratio and the polarizing capacity of these materials. However, carbonate formation at the zeolite surface during chemisorption can considerably limit CO_2 adsorption by blocking surface cations [48]. In

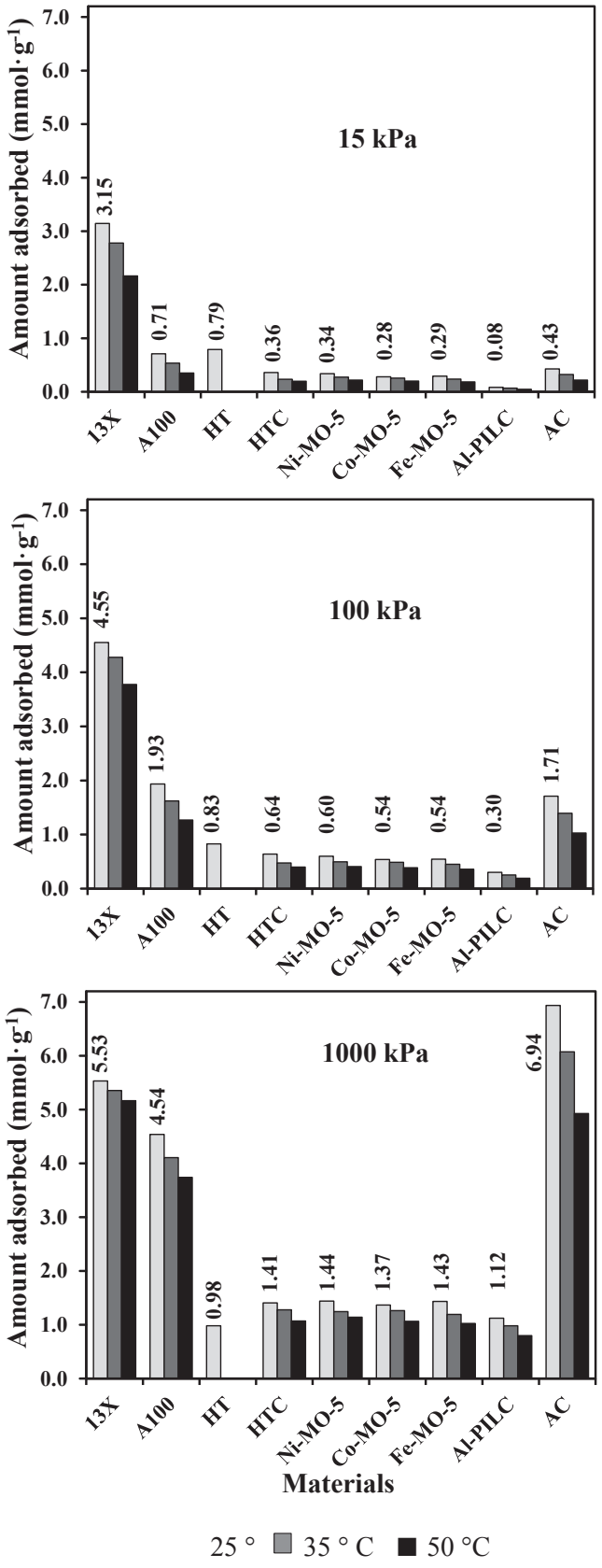

Fig. 6. CO_2 adsorption capacity at 25, 35, 50 °C and pressures of 15, 100 and 1000 kPa.

addition to the above factors, high temperatures disfavor CO_2 adsorption whereas high pressures enhance CO_2 diffusion in the zeolite, thereby improving CO_2 capture. As regards Al-PILC, it appears that the

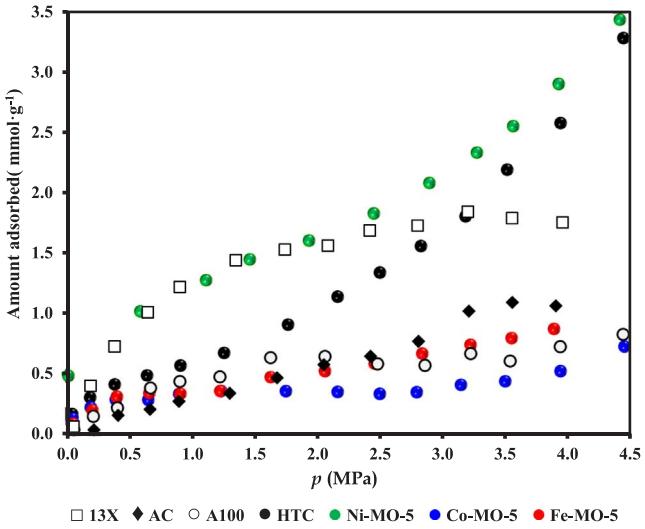

Fig. 7. CO_2 adsorption at 300 °C.

Table 2
CO_2 adsorption capacity at 300 °C.

Sample	Amount adsorbed of CO_2 (mmol·g^{-1})			
	p = 0.1 MPa	p = 1 MPa	p = 3.9 MPa	p = 4.4 MPa
HTC	0.22	0.59	2.58	3.28
Ni-MO-5	0.57	1.03	2.90	3.44
Co-MO-5	0.17	0.35	0.52	0.73
Fe-MO-5	0.12	0.33	0.87	–
13X	0.18	1.27	1.75	–
A100	0.07	0.44	0.73	0.83
AC	0.00	0.29	1.06	–
Al-PILC	0.00	0.00	0.00	0.00

adsorption capacity is more related to a physisorption mechanism in which the amount of CO_2 adsorbed is negligible, at least under the conditions studied.

In light of the data included in Table 2, Ni-MO-5 is the only material that complies with the capture-capacity conditions required for SERP systems, namely a CO_2 work capacity of about 0.3 mmol·g^{-1} at 300–500 °C and 0.01–0.1 MPa [3]. Among the hydrotalcite-derived mixed oxides, Ni-MO-5 and HTC presented the highest CO_2 adsorption at pressures higher than 3.2 MPa. In general, the adsorption capacity of these materials results from the combination of physisorption and chemisorption. As the structure of these materials contains mixed oxides and a periclase phase, the chemical interactions of CO_2 are similar to that present in MgO. The strong basic sites resulting from the presence of O^{2-} anions provide available centers at their surface that explain the high CO_2 adsorption capacity of these materials [49–52]. In MgO compounds, the strength of the basic sites is related to the type of coordination of O^{2-} ions. In the case of low-coordination O^{2-} ions, which have a high basicity, a strong interaction is formed between CO_2 molecules and carbonate species. It has been reported that in the structure type Mg-Al-MO, where MO is a mixed oxide, the density and strength of the basic surface sites depend on their composition. In the case of HTC, the density of the basic sites is high due the high Al^{3+} content in the MgO matrix, which results in surface defects that compensate the positive charge generated and the unsaturation of the $^{-}$ adjacent O^{2} ions [53]. In the case of Ni-MO-5, it is possible that the higher adsorption capacity compared to HTC could be due to the fact that incorporation of Ni^{2+} promotes the formation of CO_2 adsorption sites, as suggested by Aschenbrenner et al. [22]; CO_2 is predominantly chemisorbed in this material. In the case of Co and Fe mixed oxides, it is possible that the chemical nature of the surface of these oxides is not

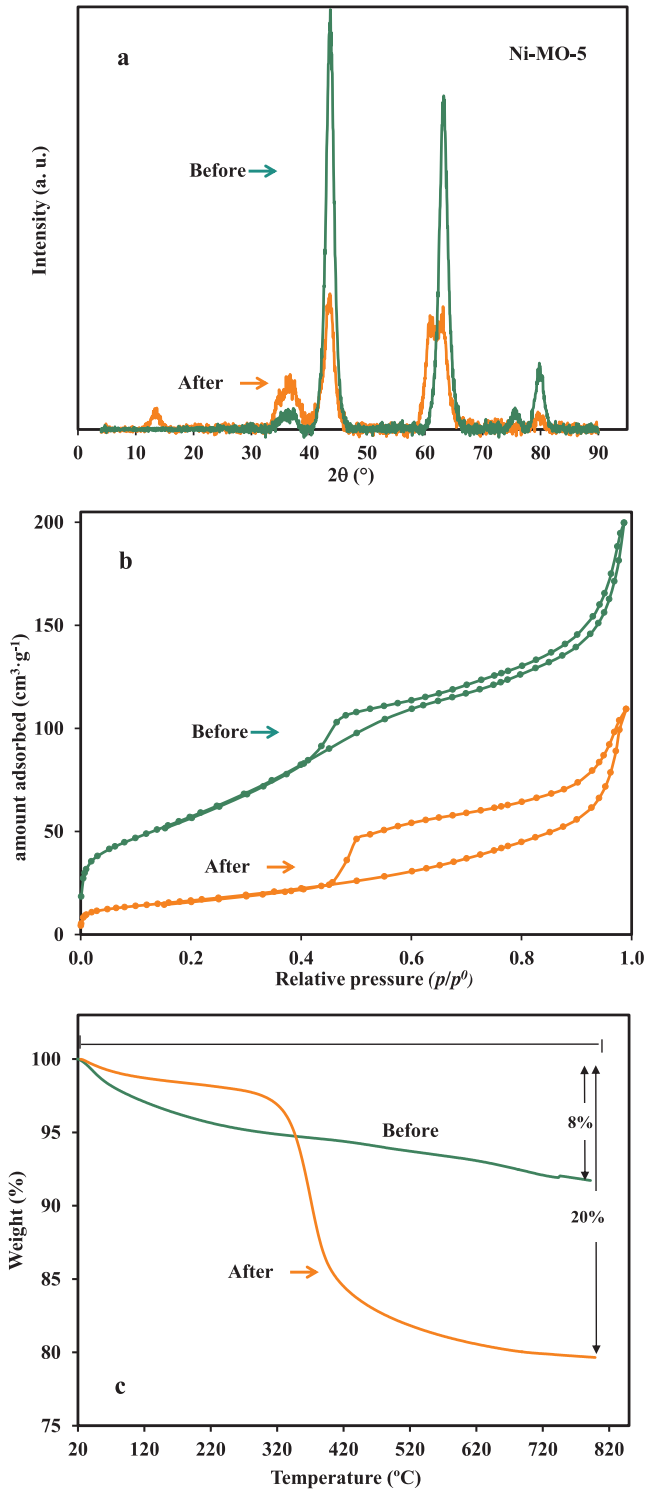

Fig. 8. Characterization results for Ni-MO-5 before and after CO_2 adsorption at 300 °C: (a) XRD patterns, (b) N_2 adsorption-desorption isotherms at −196 °C and (c) thermogravimetric analysis.

prevalent in CO_2 chemisorption and that these oxides have a lower affinity for CO_2 molecules. The amount adsorbed may be related to a physisorption process or to a lower density of active CO_2-adsorption sites. The presence of spinel structures in both materials, as it was revealed by PXRD patterns, could reduce the interaction of CO_2 molecules with the surface, and this behavior has been explained on the basis of formation of the cobalt spinel by catalytic decomposition of the initial hydrotalcite and the presence of CO_2 adsorbed as carbonate [54].

Additional characterization of the mixed oxides after CO_2 adsorption at 300 °C was performed in order to investigate possible species formation or structural changes in the materials. The results of the characterization of Ni-MO-5 are included in Fig. 8. Significant differences in the textural properties, thermogravimetric analysis and X-ray diffraction profiles were found compared to the original sample, before the adsorption. Thus, the XRD profiles (Fig. 8a) exhibit lower crystalline peaks with the presence of two new peaks at 2θ, 13° and 61°, similar to those found in the precursor sample (see Fig. 1). This suggests a partial reformation of the layered structure, or a memory effect, possibly related to the presence of carbonate species. However, these phases could not be identified by XRD analyses. CO_2 chemisorption on the surface of mixed oxides leads to the formation of various carbonate species depending on the type of basic site available for CO_2 adsorption. In the case of mixed oxides derived from hydrotalcite, the presence of various carbonate species, such as unidentate, bidentate or bicarbonates, has been described in the literature [19,43,53,55]. It can clearly be seen from Fig. 8b that CO_2 adsorption results in modification of the textural characteristics of the material. A loss of specific surface area of about 70% and a 78% decrease in total pore volume were found. This could indicate that CO_2 is chemisorbed in the mesopores, thereby blocking the mesoporosity of Ni-MO-5. A weight loss of 20% was obtained in the thermogravimetric experiments after CO_2 adsorption (Fig. 8c) and an endothermic peak (not represented in Fig. 8c) was observed at 370 °C, thus revealing the start of a possible decarbonation. The original sample shows no significant structural changes, with the observed weight loss of 8% possibly arising due to the presence of moisture or CO_2 adsorbed from the environment. In the case of HTC, the changes in the textural properties observed were a decrease of the specific surface area and total pore volume from 220 to 90 $m^2 \cdot g^{-1}$ and from 0.19 to 0.1 $cm^3 \cdot g^{-1}$ respectively, and an increase in the pore size from 3.0 to 4.6 nm. However, the XRD profiles of HTC before and after CO_2 adsorption at 300 °C and high pressures were quite similar. Concerning Co and Fe samples, no changes in textural and structural properties were found between the fresh samples and the ones used in CO_2 adsorption at 300 °C.

In summary, the above results indicate that the capacity of adsorption of Ni-MO-5 and HTC is governed by a chemisorption mechanism, due to the presence of basic sites of high strength and density.

4. Conclusions

This work has presented a quantitative and comparative study of the CO_2 adsorption capacity of Co, Fe and Ni mixed oxides derived from a commercial hydrotalcite. The materials have been characterized in terms of their physicochemical properties. The mixed oxides exhibit crystalline structures similar to the MgO pattern, as well as spinel phases. The samples can be considered to be meso-macroporous materials with specific surface areas of 200 $m^2 \cdot g^{-1}$ and mesopore sizes of 2–6 nm after thermal treatment at 500 °C.

The mixed oxides exhibit an important CO_2 adsorption capacity at 300 °C and pressures higher than 0.1 MPa up to 4.4 MPa, thus showing the potential utility of these materials in SERP schemes and post-combustion processes. Ni-MO-5 presents the best behavior, with a maximum CO_2 adsorption capacity of 3.44 $mmol \cdot g^{-1}$.

Acknowledgements

This work was funded by the Spanish State Research Agency (AEI/MINECO) and the European Regional Development Fund (ERDF) through the projects PRI-PIBAR-2011-1369 and MAT2016-78863-C2-1-R. S.I. Garcés-Polo acknowledges financial support from the Public University of Navarra through a PhD fellowship.

Appendix A. Supplementary data

Supplementary data associated with this article can be found, in the online version, at http://dx.doi.org/10.1016/j.cej.2017.09.056.

References

[1] B. Metz, O. Davidson, H.D. Coninck, M. Loos, L. Meyer, IPCC Special Report on Carbon Dioxide Capture and Storage, 2005.
[2] D.M. D'Alessandro, B. Smit, J.R. Long, Carbon dioxide capture: prospects for new materials, Angew. Chem. Int. Ed. 49 (2010) 6058–6082.
[3] J. Hufton, S. Mayorga, T. Gaffney, S. Nararaj, M. Rao, S. Sircar, Sorption enhanced reaction process (SERP) for the production of hydrogen, in: Paper presented at the Proceedings of the 1998 U.S. DOE Hydrogen Program Annual Review, Alexandria, Virginia (EE.UU.).
[4] E.R. Van Selow, P.D. Cobden, R.W. Van den Brink, J.R. Hufton, A. Wright, Performance of sorption-enhanced water-gas shift as a pre-combustion CO_2 capture technology, Energy Procedia 1 (2009) 689–696.
[5] R.W. Stevens Jr., A. Shamsi, S. Carpenter, R. Siriwardane, Sorption-enhanced water gas shift reaction by sodium-promoted calcium oxides, Fuel 89 (2010) 1280–1286.
[6] L.K.G. Bhatta, S. Subramanyam, M.D. Chengala, S. Olivera, K. Venkatesh, Progress in hydrotalcite like compounds and metal-based oxides for CO_2 capture: a review, J. Clean. Prod. 103 (2015) 171–196.
[7] R.V. Siriwardane, M.S. Shen, E.P. Fisher, Adsorption of CO_2 on zeolites at moderate temperatures, Energy Fuels 19 (2005) 1153–1159.
[8] Z. Yong, V. Mata, A.E. Rodrigues, Adsorption of carbon dioxide at high temperature—a review, Sep. Purif. Technol. 26 (2002) 195–205.
[9] B. Mu, K.S. Walton, High-pressure adsorption equilibrium of CO_2, CH_4, and CO on an impregnated activated carbon, J. Chem. Eng. Data 56 (2011) 390–397.
[10] P. Mishra, S. Mekala, F. Dreisbach, B. Mandal, S. Gumma, Adsorption of CO_2, CO, CH_4 and N_2 on a zinc based metal organic framework, Sep. Purif. Technol. 94 (2012) 124–130.
[11] R.V. Siriwardane, M.-S. Shen, E.P. Fisher, J.A. Poston, Adsorption of CO_2 on molecular sieves and activated carbon, Energy Fuels 15 (2001) 279–284.
[12] B. Spigarelli, S. Kawatra, Opportunities and challenges in carbon dioxide capture, J. CO_2 Util. 1 (2013) 69–87.
[13] C.-H. Yu, C.-H. Huang, C.-S. Tan, A review of CO_2 capture by absorption and adsorption, Aerosol Air Qual. Res. 12 (2012) 745–769.
[14] S. Wang, S. Yan, X. Ma, J. Gong, Recent advances in capture of carbon dioxide using alkali-metal-based oxides, Energy Environ. Sci. 4 (2011) 3805–3819.
[15] J. Wang, L. Huang, R. Yang, Z. Zhang, J. Wu, Y. Gao, Q. Wang, D. O'Hare, Z. Zhong, Recent advances in solid sorbents for CO_2 capture and new development trend, Energy Environ. Sci. 7 (2004) 3478–3518.
[16] S.I. Garcés, J. Villarroel-Rocha, K. Sapag, S.A. Korili, A. Gil, Comparative study of the adsorption of equilibrium of the CO_2 on microporous commercials materials at low pressures, Ind. Eng. Chem. Res. 52 (2013) 6785–6793.
[17] F. Cavani, F. Trifirò, A. Vaccari, Hydrotalcite-type anionic clays: preparation, properties and applications, Catal. Today 11 (1991) 173–301.
[18] A.L. McKenzie, C.T. Fishel, R.J. Davis, Investigation of the surface structure and basic properties of calcined hydrotalcites, J. Catal. 138 (1992) 547–561.
[19] M. León, E. Díaz, S. Bennici, A. Vega, S. Ordóñez, A. Auroux, Adsorption of CO_2 on hydrotalcite-derived mixed oxides: sorption mechanisms and consequences for adsorption irreversibility, Ind. Eng. Chem. Res. 49 (2010) 3663–3671.
[20] T. Sato, H. Fujita, T. Endo, M. Shimada, A. Tsunashima, Synthesis of hydrotalcite-like compounds and their physico-chemical properties, React. Solids 5 (1988) 219–228.
[21] X. Ge, M. Li, J. Shen, The reduction of Mg–Fe–O and Mg–Fe–Al–O complex oxides studied by temperature-programmed reduction combined with in situ mössbauer spectroscopy, J. Solid State Chem. 161 (2001) 38–44.
[22] O. Aschenbrenner, P. McGuire, S. Alsamaq, J. Wang, S. Supasitmongkol, B. Al-Duri, P. Styring, J. Wood, Adsorption of carbon dioxide on hydrotalcite-like compounds of different compositions, Chem. Eng. Res. Design 89 (2011) 1711–1721.
[23] I.O. Cruz, N.F.P. Ribeiro, D.A.G. Aranda, M.M.V.M. Souza, Hydrogen production by aqueous-phase reforming of ethanol over nickel catalysts prepared from hydrotalcite precursors, Catal. Commun. 9 (2008) 2606–2611.
[24] A. Serrano-Lotina, L. Rodríguez, G. Muñoz, L. Daza, Biogas reforming on La-promoted NiMgAl catalysts derived from hydrotalcite-like precursors, J. Power Sources 196 (2011) 4404–4410.
[25] A.F. Lucrédio, E.M. Assaf, Cobalt catalysts prepared from hydrotalcite precursors and tested in methane steam reforming, J. Power Sources 159 (2006) 667–672.
[26] A.F. Lucrédio, G. Jerkiewicz, E.M. Assaf, Cobalt catalysts promoted with cerium and lanthanum applied to partial oxidation of methane reactions, Appl. Catal. B: Environ. 84 (2008) 106–111.
[27] C. Gennequin, S. Siffert, R. Cousin, A. Aboukaïs, Co–Mg–Al hydrotalcite precursors for catalytic total oxidation of volatile organic compounds, Top. Catal. 52 (2009) 482–491.
[28] O.P. Ferreira, O.L. Alves, D.X. Gouveia, A.G. Souza Filho, J.A.C. de Paiva, J.M. Filho, Thermal decomposition and structural reconstruction effect on Mg–Fe-based hydrotalcite compounds, J. Solid State Chem. 177 (2004) 3058–3069.
[29] K.S.W. Sing, D.H. Everett, R.A.W. Haul, L. Moscou, R.A. Pierotti, J. Rouquerol, T. Siemieniewska, Reporting physisorption data for gas/solid systems with special reference to the determination of surface area and porosity (IUPAC recommendations), Pure Appl. Chem. 57 (1985) 603–6019.
[30] M. Thommes, K. Kaneko, A.V. Neimark, J.P. Olivier, F. Rodriguez-Reinoso, J. Rouquerol, K.S.W. Sing, Physisorption of gases, with special reference to the evaluation of surface area and pore size distribution (IUPAC Technical Report), Pure Appl. Chem. 87 (2015) 1051–1069.
[31] E.P. Barrett, L.G. Joyner, P.P. Halenda, The determination of pore volume and area distributions in porous substances. I. Computations from nitrogen isotherms, J. Am. Chem. Soc. 73 (1951) 373–380.
[32] D. Tichit, S. Ribet, B. Coq, Characterization of calcined and reduced multi-component Co–Ni–Mg–Al layered double hydroxides, Eur. J. Inorg. Chem. (2001) 539–546.
[33] W.T. Reichle, Synthesis of anionic clay minerals (mixed metal hydroxides, hydrotalcite), Solid State Ionics 22 (1986) 135–141.
[34] A. Parmaliana, F. Arena, F. Frusteri, N. Giordano, Temperature-programmed reduction study of NiO-MgO interactions in magnesia-supported Ni catalysts and NiO-MgO physical mixture, J. Chem. Soc. Faraday Trans. 86 (1990) 2663–2669.
[35] O. Perez-Lopez, A. Senger, N. Marcilio, M. Lansarin, Effect of composition and thermal pretreatment on properties of Ni–Mg–Al catalysts for CO_2 reforming of methane, Appl. Catal. A: General 303 (2006) 234–244.
[36] X. Yu, N. Wang, W. Chu, M. Liu, Carbon dioxide reforming of methane for syngas production over La-promoted NiMgAl catalysts derived from hydrotalcites, Chem. Eng. J. 209 (2012) 623–632.
[37] P. Arnoldy, J.A. Moulijn, Temperature-programmed reduction of CoO/Al_2O_3 catalysts, J. Catal. 93 (1985) 38–54.
[38] J. Shen, B. Guang, M. Tu, Y. Chen, Preparation and characterization of Fe/MgO catalysts obtained from hydrotalcite-like compounds, Catal. Today 30 (1996) 77–82.
[39] A. Samanta, A. Zhao, G.K.H. Shimizu, P. Sarkar, R. Gupta, Post-combustion CO_2 capture using solid sorbents: a review, Ind. Eng. Chem. Res. 51 (2012) 1438–1463.
[40] S. Choi, J.H. Drese, C.W. Jones, Adsorbent materials for carbon dioxide capture from large anthropogenic point sources, Chem. Sust. Energy Mater. 2 (2009) 796–854.
[41] N. Hutson, B. Attwood, High temperature adsorption of CO_2 on various hydrotalcite-like compounds, Adsorption 14 (2008) 781–789.
[42] N. Hutson, S. Speakman, E. Payzant, Structural effects on the high temperature adsorption of CO_2 on a synthetic hydrotalcite, Chem. Mater. 16 (2004) 4135–4143.
[43] M.K. Ram Reddy, Z.P. Xu, G.Q. Lu, J.C. Diniz da Costa, Layered double hydroxides for CO_2 capture: structure evolution and regeneration, Ind. Eng. Chem. Res. 45 (2006) 7504–7509.
[44] Z. Yong, V. Mata, A.E. Rodrigues, Adsorption of carbon dioxide onto hydrotalcite-like compounds (HTlcs) at high temperatures, Ind. Eng. Chem. Res. 40 (2001) 204–209.
[45] M.J. Ramírez-Moreno, I.C. Romero-Ibarra, M.A. Hernández-Pérez, H. Pfeiffer, CO_2 adsorption at elevated pressure and temperature on Mg–Al layered double hydroxide, Ind. Eng. Chem. Res. 53 (2014) 8087–8094.
[46] S. Cavenati, C.A. Grande, A.E. Rodrigues, Adsorption equilibrium of methane, carbon dioxide, and nitrogen on zeolite 13X at high pressures, J. Chem. Eng. Data 49 (2004) 1095–1101.
[47] A. Gil, R. Trujillano, M.A. Vicente, S.A. Korili, Adsorption of nitrogen, hydrogen and carbon dioxide on alumina-pillared clays, Stud. Surf. Sci. Catal. 160 (2007) 327–334.
[48] D. Bonenfant, M. Kharoune, P. Niquette, M. Mimeault, R. Hausler, Advances in principal factors influencing carbon dioxide adsorption on zeolites, Sci. Technol. Adv. Mater. 9 (2008) 013007.
[49] M.-L. Bailly, C. Chizallet, G. Costentin, J.-M. Krafft, H. Lauron-Pernot, M. Che, A spectroscopy and catalysis study of the nature of active sites of MgO catalysts: thermodynamic Brønsted basicity versus reactivity of basic sites, J. Catal. 235 (2005) 413–422.
[50] V.K. Díez, C.R. Apesteguía, J.I. Di Cosimo, Acid–base properties and active site requirements for elimination reactions on alkali-promoted MgO catalysts, Catal. Today 63 (2000) 53–62.
[51] J.C. Lavalley, Infrared spectrometric studies of the surface basicity of metal oxides and zeolites using adsorbed probe molecules, Catal. Today 27 (1996) 377–401.
[52] G. Ramis, G. Busca, V. Lorenzelli, Low-temperature CO_2 adsorption on metal oxides: spectroscopic characterization of some weakly adsorbed species, Mater. Chem. Phys. 29 (1991) 425–435.
[53] J.I. Di Cosimo, V.K. Díez, M. Xu, E. Iglesia, C.R. Apesteguía, Structure and surface and catalytic properties of Mg-Al basic oxides, J. Catal. 178 (1998) 499–510.
[54] X. Wang, J. Yu, J. Cheng, Z. Hao, Z. Xu, High-temperature adsorption of carbon dioxide on mixed oxides derived from hydrotalcite-like compounds, Environ. Sci. Technol. 42 (2008) 614–618.
[55] S. Radha, A. Navrotsky, Energetics of CO_2 adsorption on Mg–Al layered double hydroxides and related mixed metal oxides, J. Phys. Chem. C 118 (2014) 29836–29844.